Supplementary Information

Radiation Enhanced Uptake of $Hg^0_{(g)}$ on Iron (Oxyhydr)Oxide Nanoparticles

Uday Kurien[†], Zhenzhong Hu[‡], Heonho Lee[‡], Ashu P. Dastoor[□] and Parisa A. Ariya[*†‡]

[†]Department of Atmospheric and Oceanic Sciences and [‡]Department of Chemistry, McGill University, 801 Sherbrooke West, Montreal, QC H3A 2K6, Canada

[□] *Air Quality Research Division, Environment and Climate Change Canada, 2121, Route Transcanadienne, Dorval, QC H9P 1J3, Canada*

parisa.ariya@mcgill.ca*

*Corresponding author

S1. Method of Analysis

The GC was fitted with HP-5MS column and operated in tandem with a HP 5973 mass selective detector. The GC was operated in splitless mode with a carrier gas (ultrahigh purity Helim) flow of 1.5 mL/min. A straight design, splitless type inlet liner packed with silated glass wool was used. The injection port was maintained at 120 °C while the oven was kept isothermal at 60 °C. To check for memory effects trial runs were performed employing these conditions, however, the runs were terminated by ramping the temperature, at at 30 °C/minute, to 200 °C and maintaining it for 30 minutes. The mass selective detector was operated in the Single Ion Scanning Mode (SIMS) with m/z ratios of 202, 201, 200 and 199. Hg^0 was sampled using a 250 µL Hamilton 1825RN gas tight syringe. For each analysis 250 µL of the sample was injected into the GC-MS. Under our operating conditions, the retention time of Hg^0 was found to be *ca.* 1.4 minutes. Calibrations were performed with $Hg^0_{(g)}$ in equilibrium with $Hg^0_{(l)}$ housed in a gas tight flask, over

the concentration range of 16.07 pg/µL – 0.32 pg/µL, corresponding to 250 µL to 5 µL injections of saturated Hg vapour. Calibration curves exhibited excellent linearity ($R^2 > 0.99$).

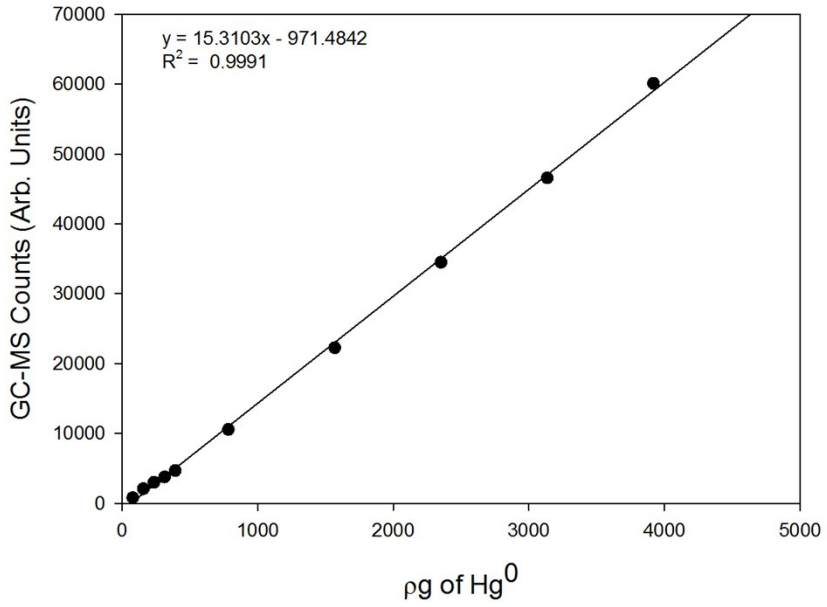

Figure S1: Sample calibration curve

S2. Characterization of Light Sources

Sanyo Denki GT15T8E, General Electronics F15T8 SP35 and Hitachi F15t8/BL were used to generate radiation in the UV-B, visible light and UV-A wavelength regions, respectively. The power of the emitted radiation was characterized using a S302C detector connected to a PM100A power meter, from Thor Labs. The S302C detector, is a thermal power sensor with an active surface area of 1.13 cm^2 and a flat response in the wavelength range of 190 nm – 25 µm. The sensor was placed at the bottom, center of the photolytic chamber with the face pointing towards the light for all measurements. It is important to note that the power measured depends on detector orientation and distance from the source. We find that the power emitted by the light sources (Table S1) are similar within limits of experimental error and hence do not expect our reactions to be biased by differences of irradiation power.

Table S1: Power characterization of irradiation sources

	Model	Mean (μW)	R.M.S (μW)	σ (μW)
Visible Light	General Electronics F15T8 SP35	211	216	46
UV-A	Hitachi F15t8/BL	197	202	43
UV-B	Sanyo Denki GT15T8E	193	199	48

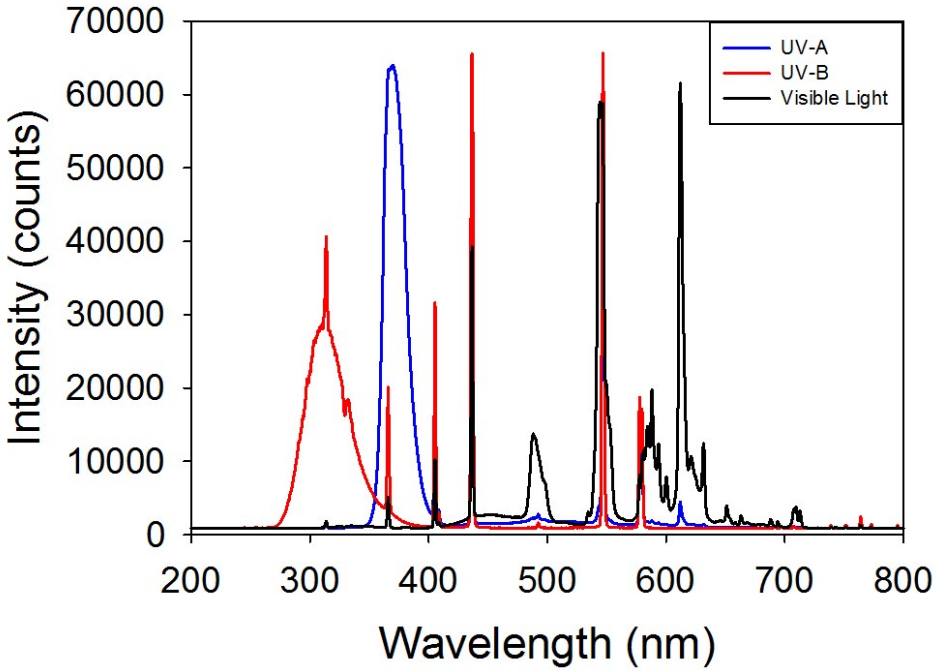

Figure S2: Emission spectra of the light sources used (Blue Lines- UV-A radiation, Red lines- UV-B radiation and Black lines- Visible light radiation)

The emission spectra of the light sources were characterized using a Jaz spectrometer from Ocean Optics connected to an Ocean Optics optical fiber (P100-2-UV/VIS) that was used as the probe. The probe was placed in the chamber and oriented in the direction of the light source. The results shown here represent the data obtain over an integration time of 7 – 10 ms averaged over 50 such collections.

For the measurement of attenuation of radiation through the flask, the S302C detector was aligned in the direction of the lightbulb of the appropriate wavelength and the power readings were

recorded. The detector was then covered with the flask, without changing its position or direction. The power of the radiation reaching the detector, through the wall of the flask, was recorded. It was observed that within limits of experimental error attenuation of UVA and visible light, through the reaction flask, was not observed however UVB radiation was attenuated by ~ 46 %.

Table S2: Characterization of attenuation of irradiation through the reaction flask

	Unobstructed radiation (μW)	**σ (μW)**	**Radiation through flask wall (μW)**	**σ (μW)**	**% Transmittance**
Visible Light	295	33	280	34	94.9
UV-A	184	31	211	33	114.6
UV-B	319	37	173	33	53..9

S3. Sources of Uncertainty

In this study we estimate a net variability of *ca.* 50 % in rate constants arising from multiple contributing factors – (a) The variation in initial Hg^0 concentration is ± 10 % (b) GC-MS peak counts exhibit a relative standard deviation of *ca.* 10 % (c) variation in warm up time of lamps and fluctuations in emitted energy density (d) the presence of water vapor even in 'dry' conditions (e) the extent of surface coating of heterogeneous phases on the flask and (f) variations in vacuum line efficiency.

S4. Hg^0 control experiments performed in dry and saturated conditions

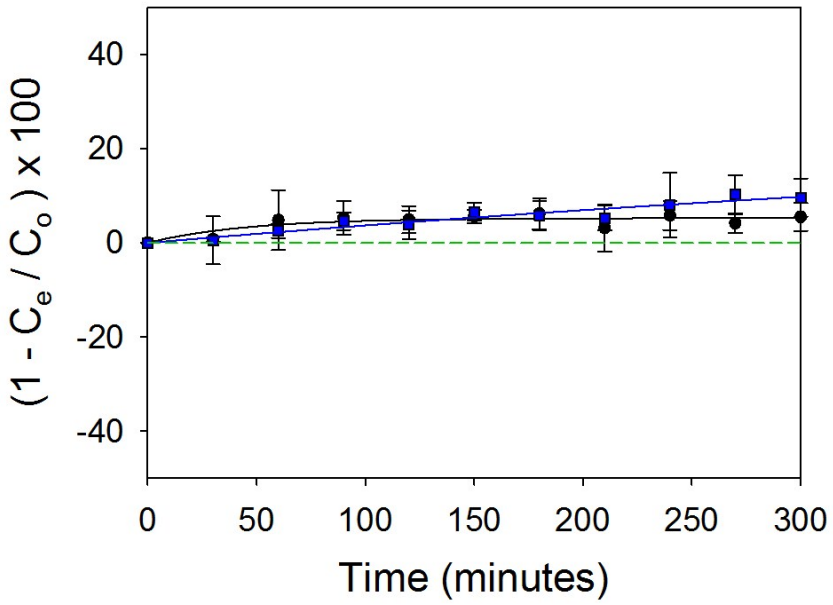

Figure S3: Control reactions performed with Hg^0 in dry (black circles) and saturated air (blue squares). The green line represents a 0 % loss of Hg^0 obtained using the initial concentration of Hg^0 at t = 0 minutes.

S5. Hg^0 control experiments in UV-A, UV-B and visible light irradiation

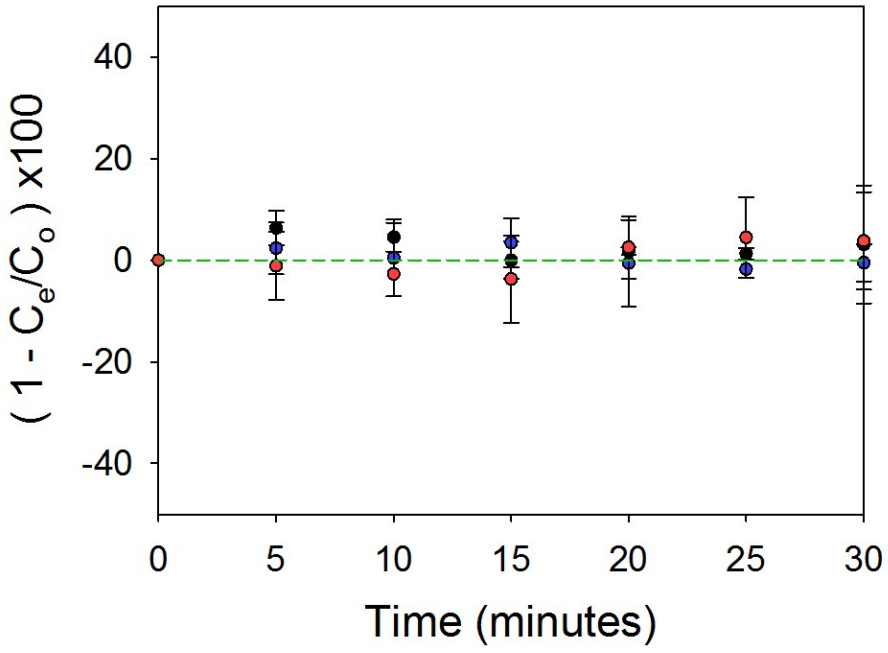

Figure S4: Effect of irradiation on Hg^0 loss in the presence of UV-A (blue circles), UV-B (red circles) and visible light (black circles) radiation. The green dashed line represents the 0 % loss of Hg^0 defined at the time of start (t = 0 minutes) of the experiment.

Radiation was impinged on the reaction flask, containing Hg^0 in dry air, in 2 pulses of 15 minutes each. The total exposure time (30 minutes) of the control reactions was equal to the total exposure time of the Hg^0 uptake reactions presented in the main text. A consistent trend for the loss of Hg^0 was not observed for the control experiments. The oscillations of Hg^0 loss relative to the starting loss (defined as 0 % at t =0 minutes, represented by the green dashed line) is a consequence of the experimental uncertainty previously discussed.

S6. Spliced curves for uptake of Hg^0 by iron oxides on irradiation

The curves shown below were obtained by plotting changes in $Hg^0_{(g)}$ concentration against irradiation time. Since $Hg^0_{(g)}$ concentrations were constant when the irradiation sources were switched off (figure 3, main text), those data points were neglected in figures S6a, S6b and S6c. The resulting figures allow for the analysis of $Hg^0_{(g)}$ loss as if under a continuous 30 minute

irradiation pulse. The rate constants for the loss of $Hg^0_{(g)}$ are easily obtained from this data by plotting $\ln[Hg]_t/\ln[Hg]_o$ as a function of time as defined by equation 2 (E2) in the main text.

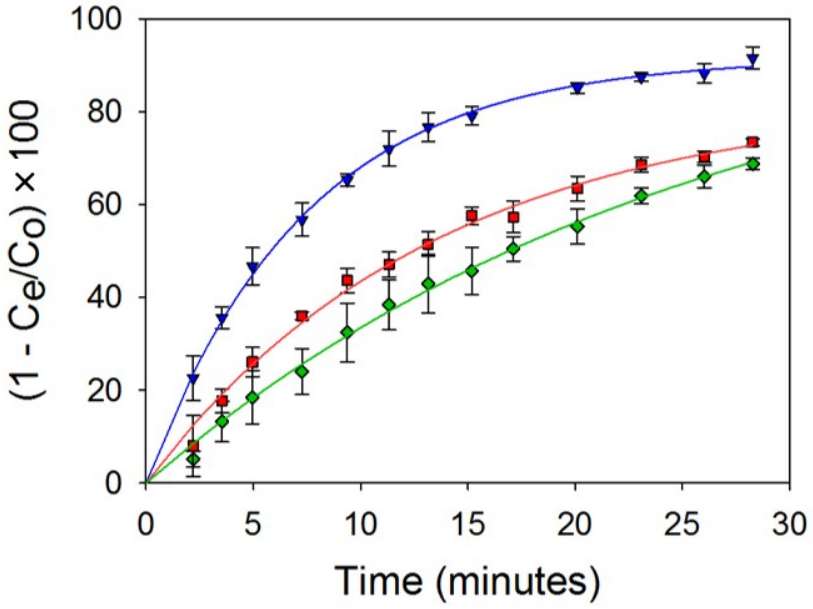

Figure S5a: Typical spliced curves for the effect of irradiation on γ-Fe_2O_3 in air (Red squares- Visible Light, Blue Inverted Triangles - UVA, Green Diamonds -UVB)

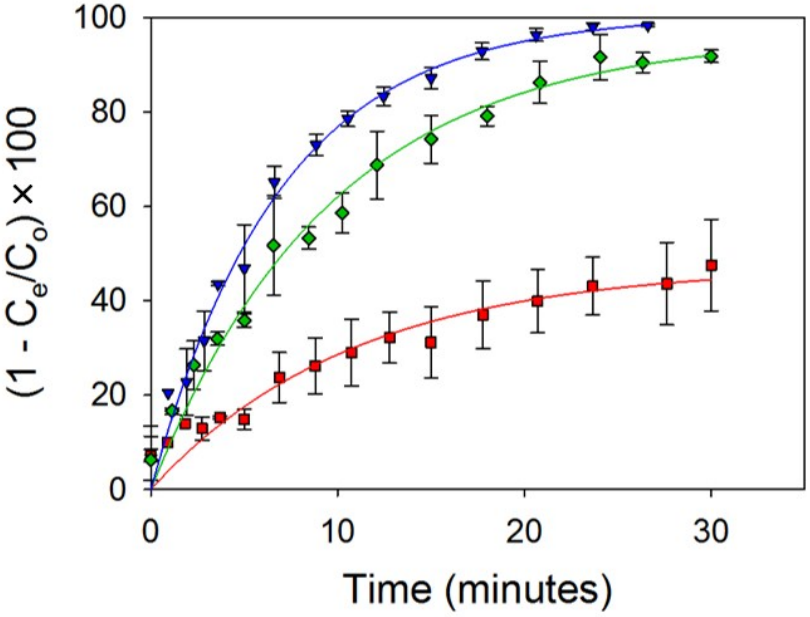

Figure S5b: Spliced curves for the effect of irradiation on the uptake of Hg^0 by α-FeOOH (Red Squares- Visible Light, Blue Inverted Triangles- UVA, Green Diamonds- UVB).

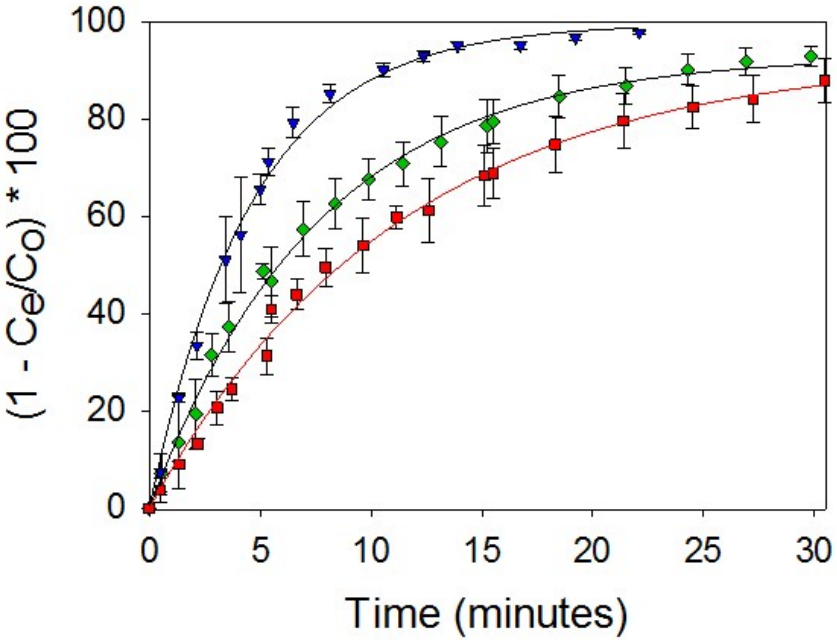

Figure S5c: Spliced curves for the effect of irradiation on the uptake of Hg^0 by α-Fe_2O_3 (Red Squares- Visible Light, Blue Inverted Triangles- UVA, Green Diamonds- UVB).

S7. UV-Vis diffuse reflectance spectra of the iron oxides and hydroxides

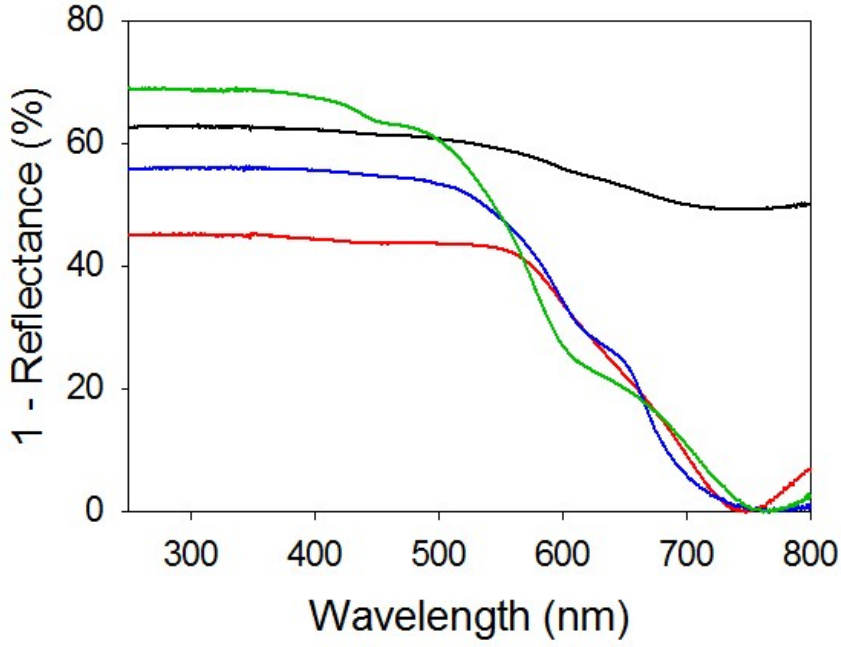

Figure S6: UV-Vis diffuse reflectance spectra of (a) Fe_3O_4 (black), (b) α-FeOOH (green), (c) γ-Fe_2O_3 (blue) and (d) α-Fe_2O_3 (red).